Modelling transport of reactive tracers in a heterogeneous crystalline rock matrix

Urban Svensson[a], Mikko Voutilainen[b,*], Eveliina Muuri[b], Michel Ferry[c], Björn Gylling[d]

[a] Computer-aided Fluid Engineering AB, Frankes väg 3, 371 65 Lyckeby, Sweden
[b] Department of Chemistry, University of Helsinki, P.O. Box 55, 00014 Helsinki, Finland
[c] MFRDC, 6 rue de la Perche, 44700 Orvault, France
[d] Gylling GeoSolutions, 3556 Davis Street, Evanston, IL 60203, USA

A B S T R A C T

A numerical reactive transport model for crystalline rocks is developed and evaluated. The model is based on mineral maps generated by X-ray micro computed tomography (X-µCT); the maps used have a resolution of approximately 30 µm and the rock samples are on the cm scale. A computational grid for the intergranular space is generated and a micro-DFN (Discrete Fracture Network) model governs the grid properties. A particle tracking method (Time Domain Random Walk) is used for transport simulations. The basic concept of the model can now be formulated as follows; "when a particle is close to a reactive mineral surface it has a certain probability to get sorbed during a certain time span. Once sorbed it will remain so a certain time". The model requires a number of input parameters that represent the sorption properties of the reactive minerals. Attempts are made to relate the parameters to traditional distribution parameters. The model is evaluated by comparisons with recent laboratory experimental data. These experiments consider two rock types (veined gneiss and pegmatitic granite) and two radionuclides (cesium and barium). It is concluded that the new reactive transport model can simulate the experimental data in a consistent and realistic way.

1. Introduction

Reactive processes in porous media take place at the interfaces between fluid and solid phases (Molins, 2015). When considering diffusive transport of radionuclides in a crystalline rock, we need to consider processes on the micrometer (µm) scale. Typically the mineral grains are larger but the aperture of micro fractures and the distances between grains are on the µm scale (Voutilainen et al., 2019a). Recently X-ray micro computed tomography (X-µCT) and related analysis methods have been developed to resolve three-dimensional grain distributions (Ketcham and Carlson, 2001; Fusseis et al., 2014). These grain maps have a resolution of about 10 µm and hence describe the grains well, but the sample size is presently limited to a few cm. Each grain can be connected to a mineral type and the abundances of the main minerals can be calculated.

It has been demonstrated (Trinchero et al., 2016; Iraola et al., 2017; Voutilainen et al., 2017; Tachi et al., 2018) that the heterogeneity of a rock matrix affects the diffusion process as, for example, manifested in a breakthrough-curve (BTC). Specific sorption on surfaces of different minerals and heterogeneities in pore and mineral structures have been suggested as an explanation to this departure from models assuming a homogeneous matrix. This study, along the studies mentioned above, is motivated by the performance assessment and safety analysis of underground repositories for spent nuclear waste. In the Swedish and Finnish programs a crystalline rock (e.g. gneiss, granite and metamorphic rock) has been chosen as the host medium and we are hence focused on migration in this type of bedrocks.

In this study, a numerical model of reactive transport will be presented and evaluated. The starting point is the three-dimensional mineral map provided by X-µCT. From such maps computational grids that cover the intergranular space are generated and grid properties are specified. The model is based on a particle tracking routine and particles will hence diffuse in the 3D intergranular grid. In this type of simulations a particle means a fraction of mass and sometimes the term tracer particle is used. If a particle is close to a reactive mineral surface it may get sorbed and stay sorbed for a certain time. It is realized that the model will entail a large number of parameters that cannot be firmly established. For this reason, we present the model more as an approach with some novel features that are still open for improvements. The reactive particle tracking method is implemented in the hydrogeological code DarcyTools (Svensson and Ferry, 2014). DarcyTools is a finite volume code that embodies a wide range of techniques and methods needed in the hydrogeological evaluation of deep repositories. In fact, DarcyTools was developed with this type of applications in mind and can hence be described as the tailor made repository code.

The construction of the computational grid is based on work performed by Voutilainen et al., 2012, 2019a using C-14-PMMA autoradiography and X-µCT. The recent ideas by Iraola et al. (2017) and

---

Please cite this article as: Urban Svensson, et al., Journal of Contaminant Hydrology, https://doi.org/10.1016/j.jconhyd.2019.103552

Svensson et al. (2018, 2019) for constructing 3D intergranular grids have been applied and further developed. Time Domain Random Walk (TDRW) has been used in the transport modelling where ideas presented by Dentz et al. (2012), Iraola et al. (2017) and Voutilainen et al. (2017) have been adapted for simulating the reactive transport of the tracer particles. Recently, Russian et al. (2016) and Kuva et al. (2019) have improved the TDRW method so that effect of advection can be taken into account.

The model will be evaluated in various ways. The main part is a comparison with some recent laboratory experiments, considering diffusion and sorption of cesium and barium (Muuri et al., 2017, 2018a, 2018b). Both veined gneiss and pegmatitic granite were used in the experiments and various distribution coefficients were evaluated. The rock samples used in the experiments were not scanned by X-µCT; so other samples from the site were used in the numerical experiments. The samples used are however from the same borehole. The model is also evaluated by relating the model parameters to the distribution coefficients (K_d and K_a, to be defined in Section 2.3) that are typically determined experimentally to represent the magnitude of chemical sorption. A comparison is also performed with a simple through diffusion case for which an analytical solution is available. The main objective of the study is to present and evaluate a reactive particle tracking method that is based on X-µCT.

2. Materials and methods

2.1. The rock samples

In the framework of the large experimental "rock matrix REtention PROperties" (REPRO) project carried out at the ONKALO test site in Finland, different laboratory characterization studies have been conducted. Two types of crystalline rock samples from the experimental site of the REPRO project are studied in this work. The selected veined gneiss (VGN) and pegmatitic granite (PGR) samples represent the typical rock types of Olkiluoto and their porosity, mineralogy and transport properties have been widely studied previously (Kärki and Paulamäki, 2006; Smellie et al., 2014; Ikonen et al., 2014; Kuva et al., 2015; Sammaljärvi et al., 2017; Muuri et al., 2018b; Voutilainen et al., 2018; Aromaa et al., 2019). The samples represent the same rock types and have been collected from the same drill cores (PGR samples from ONK-PP318 and VGN samples from ONK-PP323, ONK-PP324 and ONK-PP327) as the samples for the laboratory experiments (See Section 2.2). In previous studies, porosities ranging from 0.3% to 0.75% and from 0.3% to 1.3% have been measured for PGR and VGN, respectively, samples from the REPRO site using water gravimetry, Ar-gas pycnometry and C-14-PMMA autoradiography (Ikonen et al., 2014; Kuva et al., 2015). Furthermore, effective diffusion coefficients of $(5.7 \pm 0.7) \times 10^{-13}\,\mathrm{m^2/s}$ and $(1.7 \pm 0.2) \times 10^{-13}\,\mathrm{m^2/s}$ were measured for PGR and VGN, respectively, samples using through- diffusion experiments of HTO (Voutilainen et al., 2018). Voutilainen et al., 2019b have estimated that in in situ conditions the porosities and effective diffusion coefficients are about 20% and 32%, respectively, smaller than in the laboratory experiments indicate.

Previously, Voutilainen et al., 2019a have resolved the 3D mineral structure of the REPRO samples with X-Ray tomography and determined the porosity distribution with C-14-PMMA autoradiography. Furthermore, they have constructed 3D grain distributions of the samples by first segmenting different main mineral phases from each other by their X-ray attenuation coefficient and then grains from mineral phases by performing a watershed segmentation on 3D mineral phase images. The main minerals of the samples are quartz, plagioclase, K- feldspar and mica. Unfortunately, the X-ray attenuation of quartz and plagioclase overlap, and thus they cannot be segmented from each other directly. However, the grains belonging to the mineral phase that included quartz and plagioclase were randomly divided according to their known abundances (Sammaljärvi et al., 2017). The constructed 3D
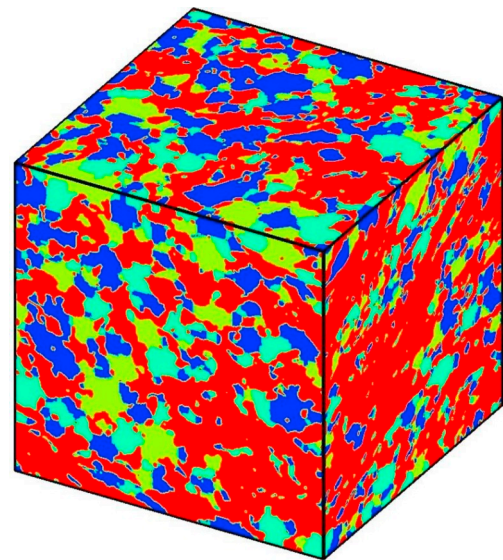
VGN
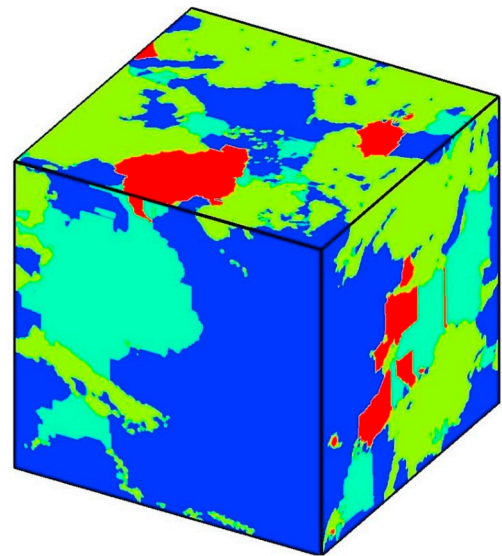
PGR

Fig. 1. Three-dimensional visualisation of the two considered rock samples after mineral segmentation. The size of samples is $1\,\mathrm{cm^3}$. The mineral phases shown are: quartz (blue), plagioclase (green), K- feldspar (yellow) and mica (red). (For interpretation of the references to colour in this figure legend, the reader is referred to the web version of this article.)

grain distributions (see Fig. 1) form the base of this work and are being further processed in order to create more realistic grain scale models. The 3D grain distributions were 8-bit gray scale images. The gray scale values of each grain were artificially selected so that different minerals had their own gray scale range and no grain has the same gray scale value as any of its neighboring grains (see Table 1). Furthermore, the voxel size of the original 3D grain distributions was reduced to $27.16\,\mu m$.

2.2. The laboratory experiments

The laboratory diffusion experiments used for the evaluation of the model are described in detail by Muuri et al., 2017, 2018a, 2018b. Two diffusion experiments with different set- ups were carried out (see Fig. 2). In the first type of experiment, (Muuri et al., 2017, 2018a) a

Table 1
The analyzed mineral abundances of the VGN and PGR samples and the artificial gray value indexes used in the 3D grain distributions.

Rock	Mineral	Vol (%)	Grain map index
VGN	Quartz	28	40–52
	Plagioclase	14	100–112
	K-feldspar	16	120–132
	Mica minerals	42	60–72
PGR	Quartz	46	20–32
	Plagioclase	21	100–112
	K-feldspar	31	41–53
	Mica minerals	2	60–72

cube, approximately $1 \times 1 \times 1 \, cm^3$, was placed at the bottom of a vessel and five faces of the cube were exposed to the tracer solution (volume of 15 ml). Results for cesium were reported in Muuri et al. (2017) and results for barium in Muuri et al., 2018a. In the second type of experiment (Muuri et al., 2018b), diffusion of barium was studied using a larger sample ($4.5 \times 3 \times 1 \, cm^3$), Fig. 2.

Only one side was exposed to the solution (volume of 20 ml) in order to allow one-dimensional models in the analysis. In practice, this is equivalent with case where solution is transported in water conducting fracture and the tracer molecules may diffuse to surrounding rock matrix. The phenomena is the main retention process for the transport of radionuclides in bedrock (Posiva, 2013). For both experiments two rock types were tested; VGN and PGR, while in the second experiment the surface was polished after sawing; in the first experiment it was not. Muuri et al., 2018b performed the polishing to determine accurately the penetration curves after the diffusion experiment and it can be assumed that the polishing does not affect the decrease of the tracer concentration.

The decrease of the tracer concentration in the solution, $C(t)$, was measured during the experiment. In the analysis, $C(t)$ is scaled using the initial concentration of the tracer in the surrounding solution, C_0, in order to compare different measurements. In the first experiment $C(t)$ was measured for four months and in the second experiment $C(t)$ was measured for about three months. The numerical model is set up to simulate the experimental data and conditions as closely as possible. Another useful result from the experiments was the K_d values obtained from crushed minerals and rocks. Our model is built on the concept that each tracer sorbs on one or several specific minerals. From the experiments mineral specific K_d values were measured. It is expected that these are correlated to the adsorption time, T_d, which is an important model parameter. The correlation will be evaluated.

2.3. Transport model

A conceptual view of the situation considered is given in Fig. 3. Initially all particles are in solution and we denote this concentration C_0. It is then expected that particles will sorb on mineral surfaces that are directly exposed to the solution. This is a comparatively fast process as the molecular diffusion of the solution controls the time scale. Particles may also diffuse into the rock through intergranular micro fractures and sorb on internal surfaces; hence an in-diffusion process, which is slower as the effective intergranular diffusion coefficient is lower than the molecular diffusion coefficient for the solution. A global parameter of interest is the decreasing concentration, $C(t)$, in the solution normalized with the initial concentration, i.e. $C(t)/C_0$.

The basic concept of the numerical model presented here is that different radionuclides react differently with different mineral surfaces. As an input the model requires a three-dimensional mineral map and information how a certain radionuclide reacts with different minerals. Note that this is not information that is provided by the traditional distribution coefficients K_d and K_a.

The basic parameters of the model can now be introduced. When a

particle is "close" to a reactive mineral surface, it has a certain probability, P_s, to get sorbed within a certain time interval, T_s. If sorbed, it will stay sorbed for a time, T_d, before desorption. An immediate question is what "close" means. We are developing a numerical method and it will be assumed that a particle may get sorbed when in a computational cell that has one or more cell faces in contact with a reactive grain. The cell size, Δ, is hence a model parameter. If we consider that the events of being sorbed are distributed according to an exponential density function with parameter k_1, then.

$$F(X) = exp.(-k_1 * X) \quad if X \geq 0$$
$$F(X) = 0 \qquad\qquad\quad if X < 0 \tag{1}$$

where X is a continuous random variable.

Then the probability P_s that the particle gets sorbed before T_s is given by:

$$P_s = P(X \leq T_s) = 1 - exp.(-k_1 * T_s) \tag{2}$$

which gives:

$$k_1 = -Log(1 - P_s)/T_s \tag{3}$$

Now consider that the desorption events are distributed according to an exponential density function (assuming that the time between events is a Poisson point process) with parameter k_2. The mean time before release is then given by:

$$T_d = E(X) = 1/k_2 \tag{4}$$

where

$$k_2 = 1/T_d \tag{5}$$

k_1 and k_2 are the numerical input parameters of the model.

When setting the numerical values for the four parameters (P_s, T_s, T_d and Δ) one should note that they are related, see Appendixes A and B. The cell size is considered as fixed and T_d will be a calibration parameter and we hence need to set values for P_s and T_s:

- P_s. If one out of six cell walls is in contact with a sorbing mineral the probability to get sorbed is 1/6. However, more cell walls can be in contact and we chose to put $P_s = 0.2$.
- T_s. The time to leave a cell by molecular diffusion is specified for $T_s (= (\Delta/2)^2/D_{mol})$, where D_{mol} is the molecular diffusion coefficient.

It should be emphasized that the exact values chosen for P_s and T_s will influence T_d, see discussion section. One may also note that P_s and T_s are both part of (3); strictly only three parameters are needed. However, we keep both P_s and T_s for easier physical interpretation.

The particle tracking method is Time Domain Random Walk (TDRW) (Russian et al., 2016). The method is implemented for both advection and diffusion in the code used (DarcyTools, Svensson and Ferry, 2014), but here only diffusive transport is considered. DarcyTools is a finite volume code for simulation of flow and transport in porous and/or fractured media. It is a general code for this class of problems, but the analysis of a repository for nuclear waste is the main intended application. Two features of the code are specifically significant in the present context; an unstructured cartesian grid with the possibility to remove/refine cells locally and grid properties that are generated from a micro-DFN.

2.4. Grids and micro-DFN

The construction of the computational grid and the intergranular fracture network (micro-DFN) are presented and discussed in detail by Svensson et al. (2019), and only described here briefly. The basic idea of the construction is outlined in Fig. 4. A grid that covers the 3D domain is first generated. The cells inside grains are removed and a grid with typically two cells covering the intergranular space is obtained. A micro-DFN, with fracture centres inside the grid, is generated and the
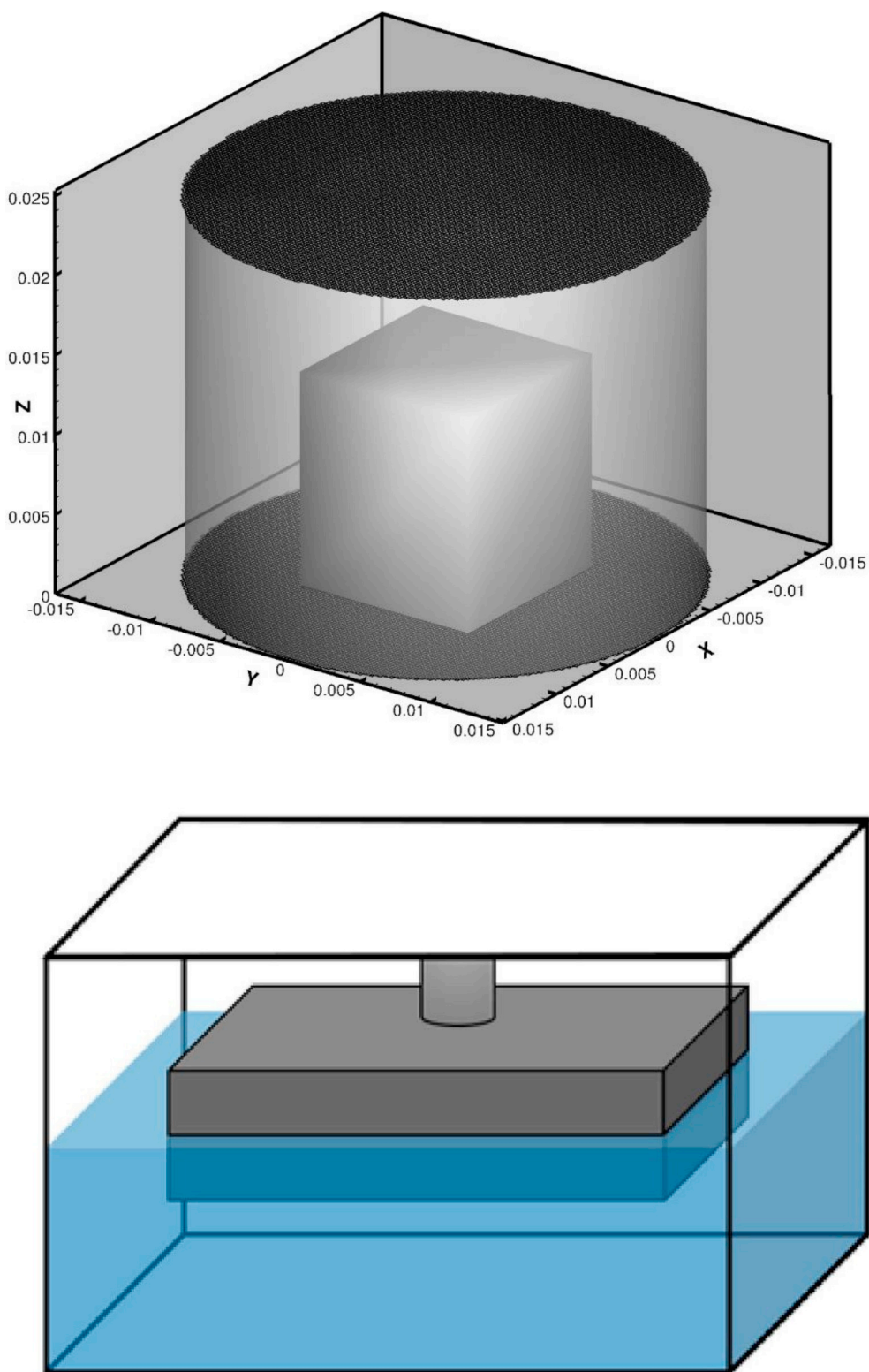
Fig. 2. The experimental set-ups. In the experiments by Muuri et al., 2017, 2018a five faces of a cube are exposed to the solution (top). In the experiments by Muuri et al., 2018b only one side is exposed to the solution. In both cases the decrease of concentration in the solution is measured.

fracture properties govern the cell properties. The cells that are not in contact with the fractures are removed, as a final step.

In the micro-DFN model, fracture orientation follows a Fisher distribution (here a random orientation is used) and spatial centres are statistically independent and follow a Poisson process. The number of fractures in the length interval l to $l + dl$ is simulated using the following power-law equation:

$$n = I \frac{l}{a} \left[\left(\frac{l + dl}{l_{ref}} \right)^a - \left(\frac{l}{l_{ref}} \right)^a \right]$$

(6)

where n is the number of fractures per unit volume, I $\lceil_{\lfloor} m^{-3} \rceil_{\rfloor}$ is the intensity, a $[-]$ is the power law exponent and l_{ref} [m] is the reference

U. Svensson, et al.
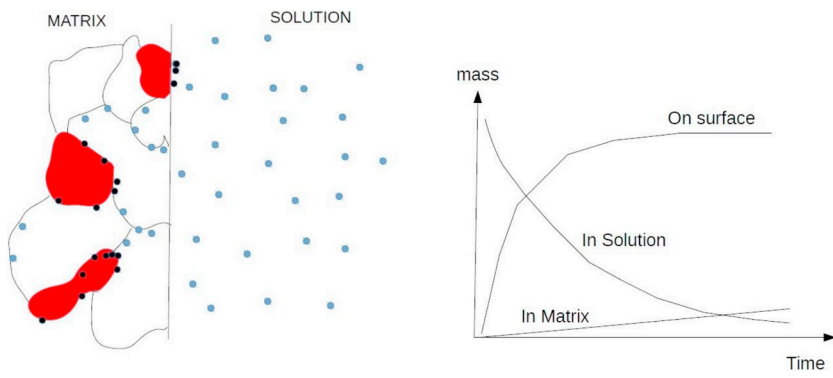
Fig. 3. A conceptual representation of the model. All particles are initially in the solution. At a later stage some particles are sorbed on reactive minerals (red); first on mineral surfaces exposed to the solution, later in the matrix. Sorbed particles are marked as black and mobile as blue. The right figure illustrates how the total mass is expected to be distributed as a function of time. (For interpretation of the references to colour in this figure legend, the reader is referred to the web version of this article.)
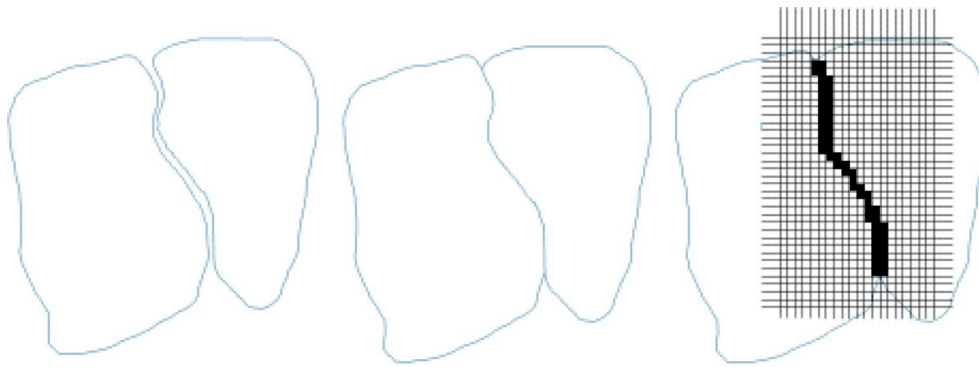
Fig. 4. An illustration of the concepts and methods that were used to create the computational grids. The intergranular region (top left) is expected to have a spacing of 1–10 μm. X-ray data does not resolve this (top middle). The shaded cells (top right) constitute the starting point of the computational grid. In the next step a micro DFN is generated, with fracture centres inside the grid. In the final step cells not in contact with the fractures are removed (shaded cells in bottom right figure). Red line in the bottom figures indicates grain boundaries and the black lines indicate fractures. Further details of the method is given by Svensson et al. (2019). (For interpretation of the references to colour in this figure legend, the reader is referred to the web version of this article.)
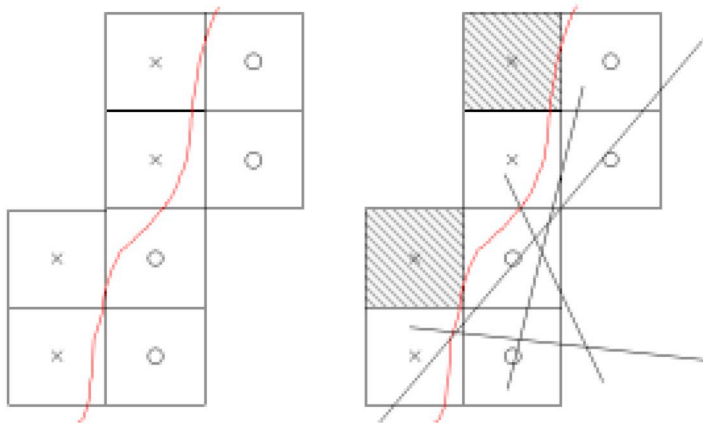
Table 2

Global properties, *De* and *ε*, as calibrated to experimental data from (Voutilainen et al. (2018a and b), Kuva et al. (2015)). The properties of the micro DFN (Table 3) are used as calibration parameters.

Rock	Calibrated		Experimental	
	$De \times 10^{-13}\,\mathrm{m^2/s}$	ε [%]	$De \times 10^{-13}\,\mathrm{m^2/s}$	ε [%]
VGN	2.5	0.58	1–2	0.3–1.3
PGR	5.5	0.60	5–7	0.3–0.75

Table 3

Micro-DFN parameters. A power law is used to generate the micro-DFN. Common for both VGN and PGR: length interval (50 → 100 μm), power law coefficient (−2.6) and random orientation.

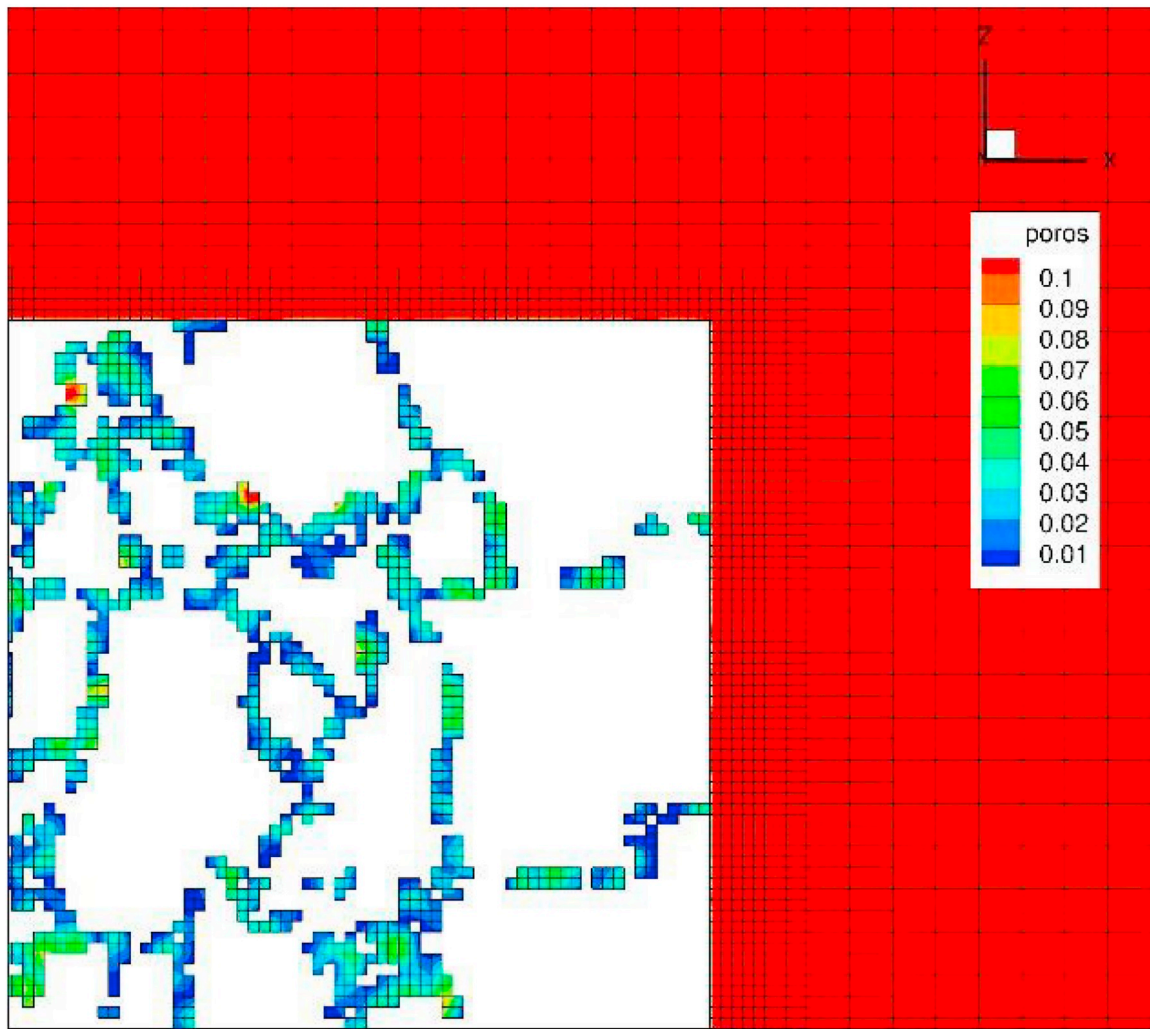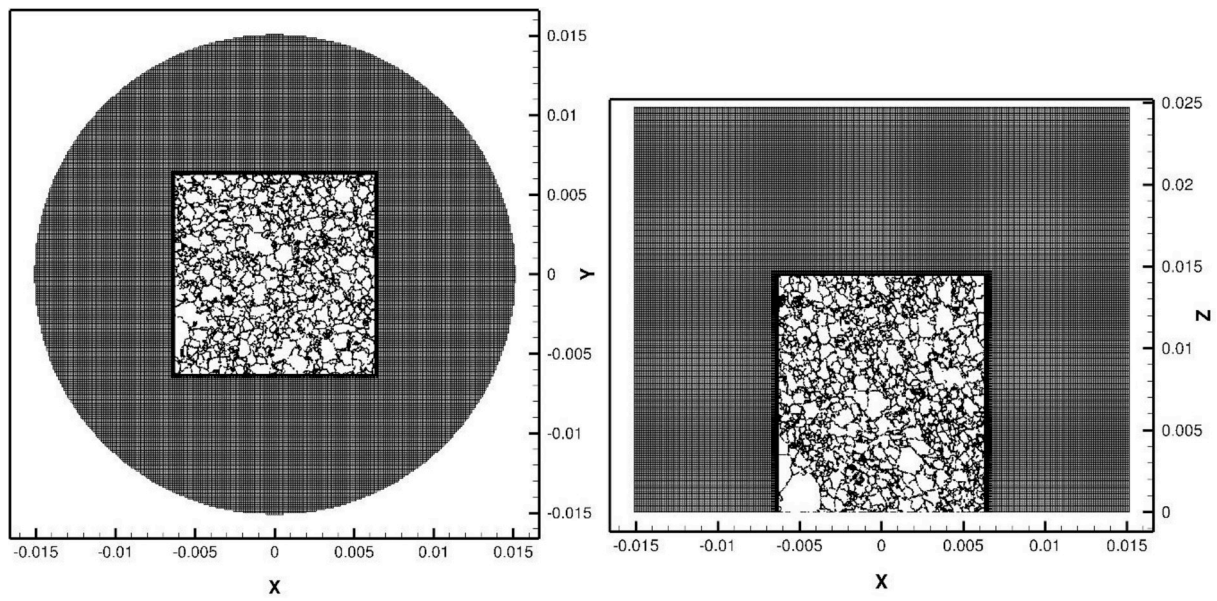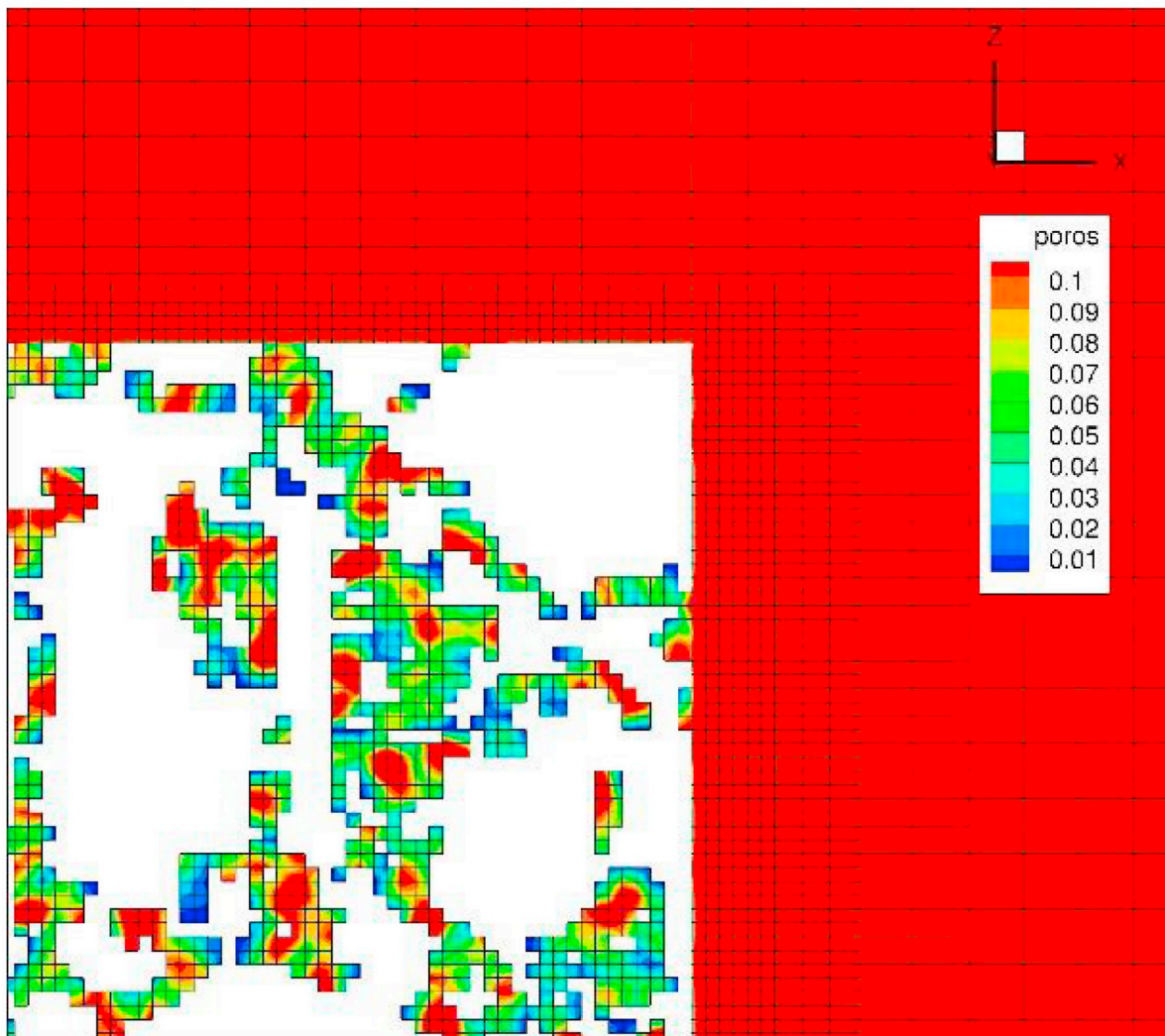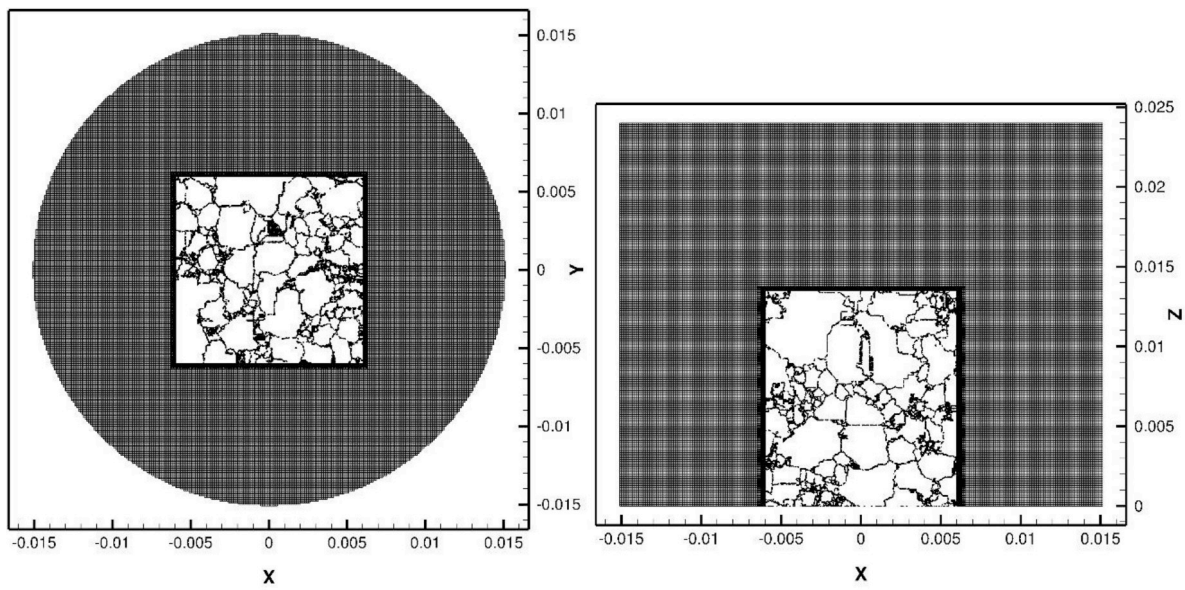| Property	VGN	PGR
Diffusion coefficient $(\mathrm{m^2/s}) \times 10^{-10}$	2.0	9.0
Aperture (μm)	1.2	2.8
Intensity $(1/\mathrm{m^3})$	100	100

Fig. 5. The computational grid for VGN and for experimental set-up according to Muuri et al., 2017, 2018a. The lower figure is an enlargement of the top right figure. The porosity field is illustrated by colours.

Fig. 6. The computational grid for PGR and for experimental set-up according to Muuri et al., 2017, 2018a. The lower figure is an enlargement of the top right figure. The porosity field is illustrated by colours.
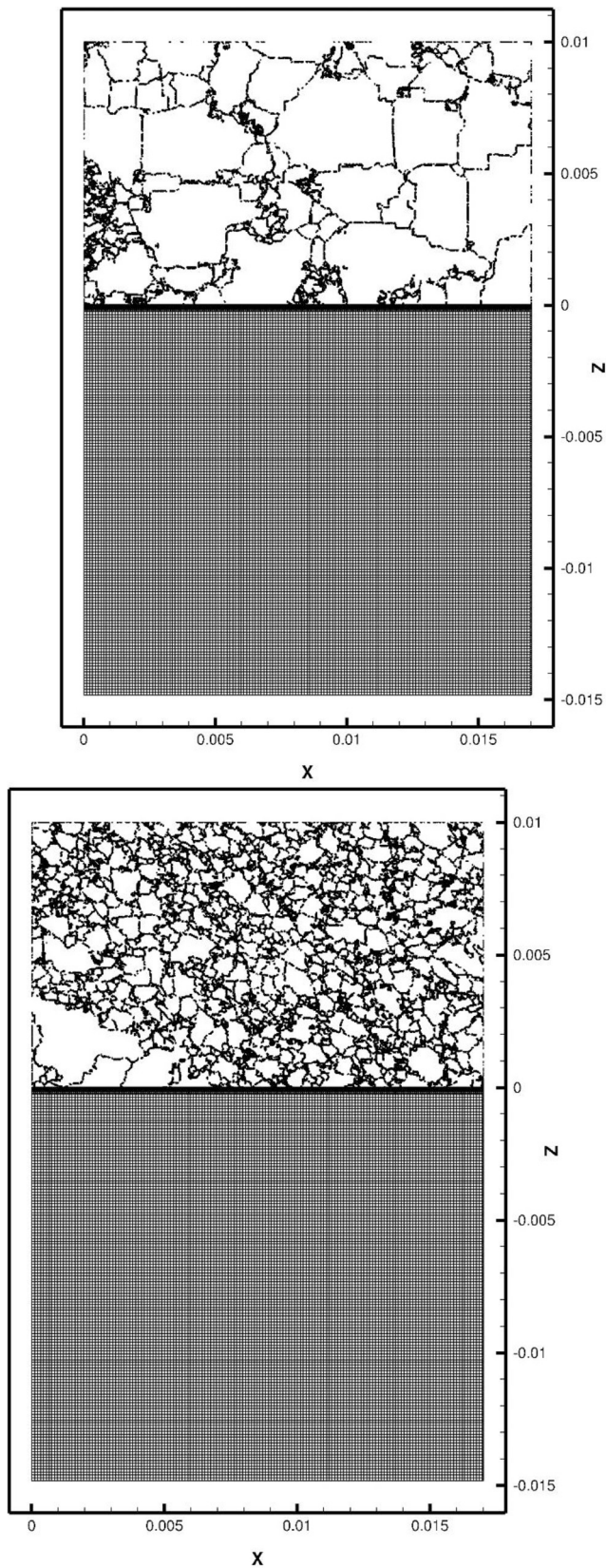
U. Svensson, et al.

Fig. 7. The computational grids for VGN (top) and PGR (bottom). Experimental set-up according to Muuri et al., 2018b.
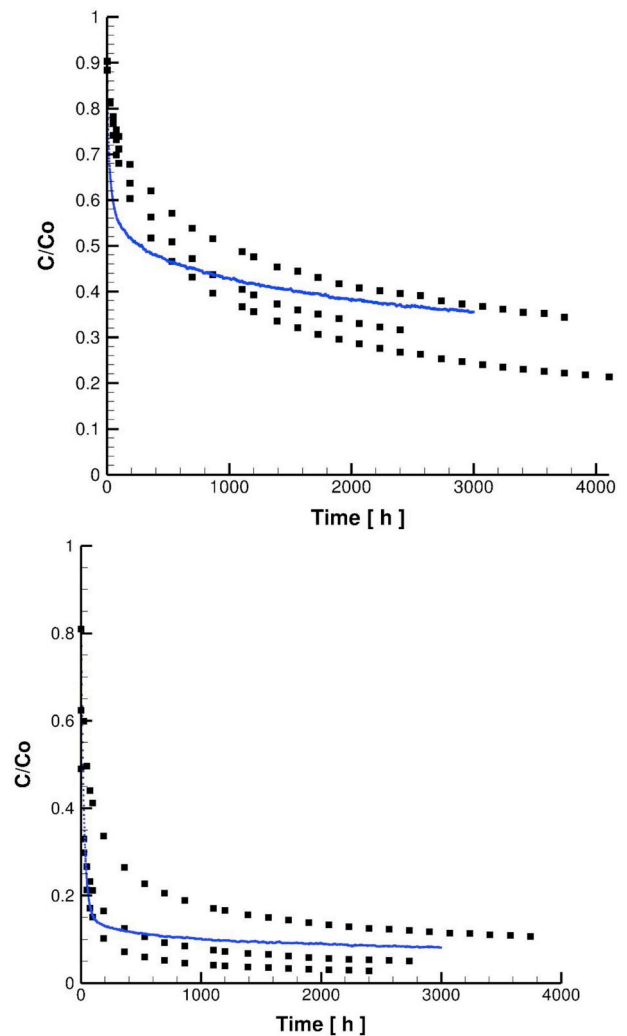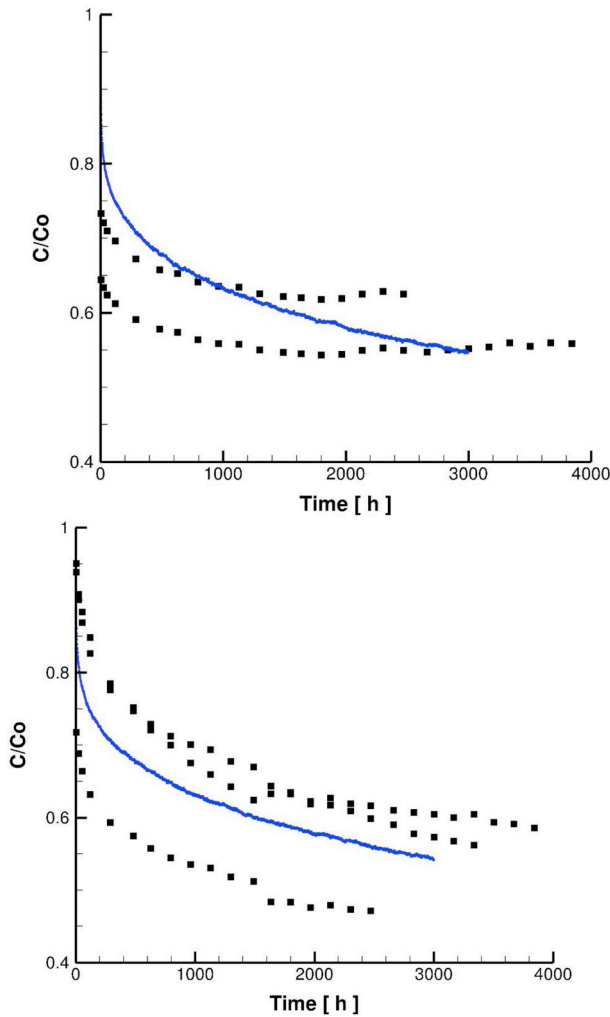

Fig. 8. A comparison of measured (squares) and simulated (solid line) concentration decrease of cesium in solution for first case considered. Three different samples were used in the experiment (Muuri et al., 2017). VGN (top) and PGR (bottom).

length, which is here set to 1 m. The micro-DFN is tuned by a simulation of a steady state through-diffusion case, with fixed upstream and downstream boundary conditions. The flux through the sample then gives the effective diffusion coefficient, D_e, and the summed up intergranular porosity gives the global porosity, ε. Tables 2 and 3 give the outcome of this exercise. The tuning of the micro-DFN is discussed in Svensson et al. (2018). Here we follow the same procedure and use the diffusivity and aperture as calibration parameters. It is useful to note that the apertures will control the global porosity, while the product of the diffusivity and aperture controls the effective diffusivity. As can be seen, the calibrated D_e and ε are in agreement with experimental data. After this calibration the properties of the samples, i.e. D_e and ε, will not be changed.

Computational grids for the two experimental set-ups are shown in Figs. 5 to 7. Inside and close to the samples the grid has a constant cell size of 27.16 μm, outside this volume the grid size is expanded in order to reduce the total number of cells. Still the number of cells ranges from 15 to 42 million cells. In Figs. 5 and 6, the porosity distribution is illustrated. One may note that the PGR sample has higher intergranular porosities, which is due to the larger aperture specified for PGR, see Table 3.
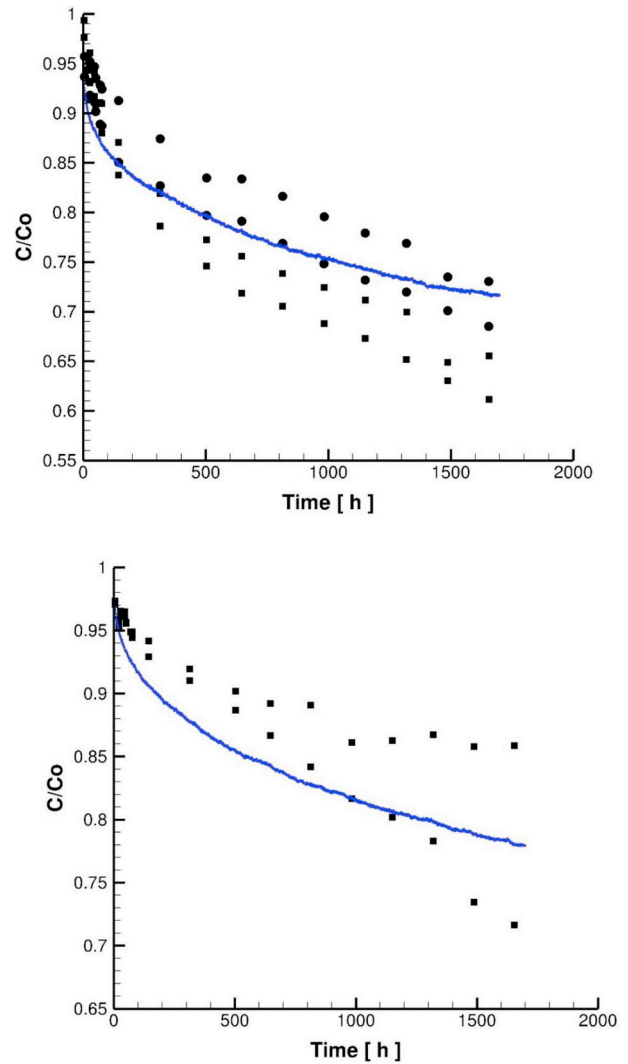
The above descriptions of data, concepts and methods are summarized by the following computational steps.

Fig. 9. A comparison of measured (squares) and simulated (solid line) concentration decrease of barium in solution for first case considered. Three different samples were used in the experiment (Muuri et al., 2018a). VGN (top) and PGR (bottom).

Fig. 10. A comparison of measured (squares) and simulated (solid line) concentration decrease of barium in solution for second case considered. Two different samples were used in the experiment (Muuri et al., 2018b). VGN (top) and PGR (bottom). In the top figure circles represent a case with diffusion perpendicular to the foliation direction and squares along the foliation. In the simulated case, the foliation was at an angle and hence in between.

1. The 3D mineral maps are the starting point. A 3D grid that covers the rock sample is generated and all cells get a gray scale value.
2. Cells inside grains are removed, based on a test of gray scale values. If all neighboring cells have the same value, the cell can be removed.
3. The resulting grid has holes (representing grains) and typically two cells will cover the intergranular space, see Fig. 4.
4. Next a micro-DFN is generated with fracture centres inside the grid. The fracture network is based on Eq. (6) and the parameters in Table 3.
5. A new grid is generated. Inside the rock samples all cells not in contact with the micro-DFN are removed. Note that the mineral maps are not used at this stage. The resulting grid will have holes (representing grains) as before but a grain will no longer have a cell layer completely embedding the grain, i.e. the grid is less connected. We also note (see Fig. 4) that fractures may intersect grains and a certain intragranular space is generated.
6. Cells will get properties (diffusion coefficients and porosities) from the micro-DFN.
7. The grid is then marked with the 3D mineral map, which means that all cells get a gray scale value. Cells that belong to a reactive mineral phase are given a certain T_d value; other cells will get $T_d = 0$. It is the rates k_1 and k_2 (Eqs. (3) and (5)) that are specified for each cell.
8. The initial particle distribution is generated by a random process, giving a more or less (depending on the number of particles)

uniform distribution in the solution.
9. The TDRW can be started.

3. Results

The simulations were set up following the outlines given in Fig. 2. However, some differences should be mentioned; in the studies by Muuri et al., 2017, 2018a experiments with three different samples were performed. The samples had slightly different dimensions (the weight was from 4.9 to 5.5 g), which however is not expected to influence the results. In the present simulations an average size was used. In the study by Muuri et al., 2018b the sample was larger than the grain map available. The sample in the simulations had, for this reason, an area of 17 × 17 mm, facing the solution. The volume of the solution was adjusted correspondingly.

The model has one calibration parameter: T_d. For each case a range of values for T_d was tested and the best fit was selected. This was done subjectively without any objective criterion. In Fig. 8 the results for cesium are shown for VGN and PGR. It will be assumed that cesium sorbs only on mica for VGN. For PGR the mica content is only 2%
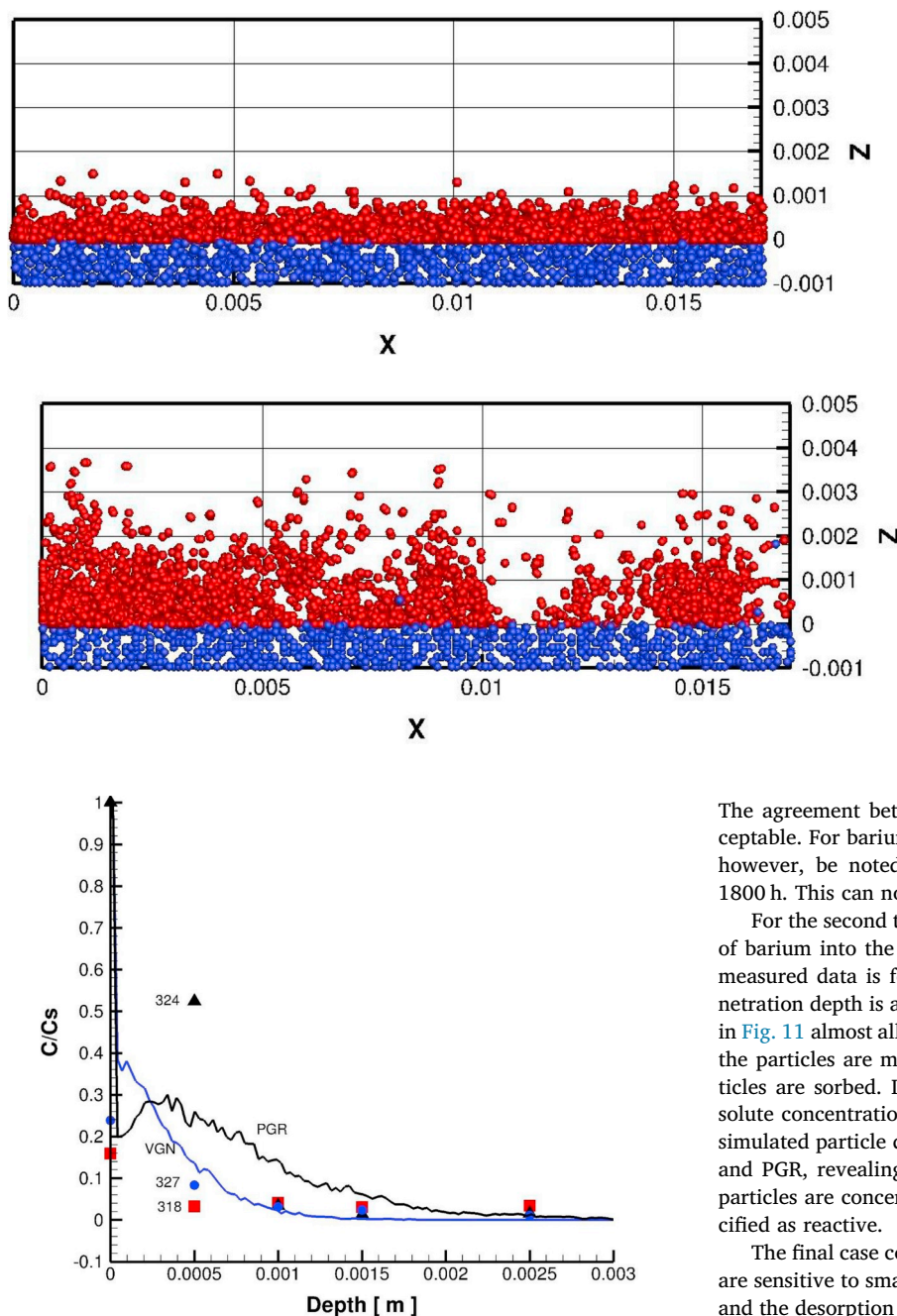
Fig. 11. Penetration of barium into VGN (top) and PGR (bottom) after 1700 h. Red particles are sorbed and blue particles are mobile. Set-up from Muuri et al., 2018b. Note that only 1 mm of the solution part is shown and heterogeneous particle distribution is caused by location reactive minerals. (For interpretation of the references to colour in this figure legend, the reader is referred to the web version of this article.)

Fig. 12. Simulated penetration of barium into VGN (blue curve) and PGR (black curve), as compared to experimental data points (318 PGR, 327 and 324 VGN). Note that Cs here means concentration of barium on the surface. (For interpretation of the references to colour in this figure legend, the reader is referred to the web version of this article.)

(Table 1) and it will be assumed that plagioclase and K-feldspar provide the sorbtion sites. For most cases both the data and the simulations show a rapid drop of concentration in the beginning followed by a slower decrease of the concentration. The first is caused by sorption on surfaces that are in contact with the tracer solution, while the slower process is due to in-diffusion, see Fig. 3. Further, the large initial drop for VGN is related to the high mica content of this sample. The corresponding results for barium are shown in Fig. 9 for the first type of experiment and in Fig. 10 for the second type of experiment. For barium the same assumption as for cesium will apply, i.e. sorbtion on mica for VGN and sorption on K-feldspar and plagioclase for PGR. Both the data and the simulation show similar concentration changes as for cesium.

The agreement between simulations and data is considered to be acceptable. For barium in VGN (Fig. 9) a less good fit is found. It should, however, be noted that the measured concentrations increase after 1800 h. This can not be captured by the model.

For the second type of experiment, an illustration of the penetration of barium into the sample is given by Fig. 11 and a comparison with measured data is found in Fig. 12. We find that after 1700 h the penetration depth is about 1 mm for VGN and 2–3 mm for PGR. Note that in Fig. 11 almost all particles are sorbed in the matrix. The time fraction the particles are mobile is hence short compared to the time the particles are sorbed. It has been argued that the fast initial drop of the solute concentration is due to surface sorption. In Figs. 13 and 14 the simulated particle distribution on the sample surface is shown for VGN and PGR, revealing surface sorption, as expected, indicating that the particles are concentrated on the mineral surfaces that have been specified as reactive.

The final case concerns a sensitivity study, shown in Fig. 15. Results are sensitive to small changes in both the effective diffusion coefficient and the desorption time. Experimentally determined effective diffusion coefficients may vary significantly. The variation shown may thus be interpreted as the effect of using a range of samples, similar to what was done in the experiments. The desorption time can be related to K_d and one may note that K_d values determined in experiments have rather high uncertainties.

The calibrated T_d values are summarized in Table 4 and will be discussed below. A nice feature of the experiments is that several samples were used for the same rock and the same tracer. The samples are from the same borehole and the spread in the results thus indicates that variations from one sample to another may still be significant. The spread also gives an uncertainty range, when it comes to comparisons with the simulated profiles. With this as a background we may conclude that the simulations are in fair agreement with the experimental data.

4. Discussion

In typical applications K_d is used as the parameter that describes the retention caused by reversible chemical sorption. For this reason we
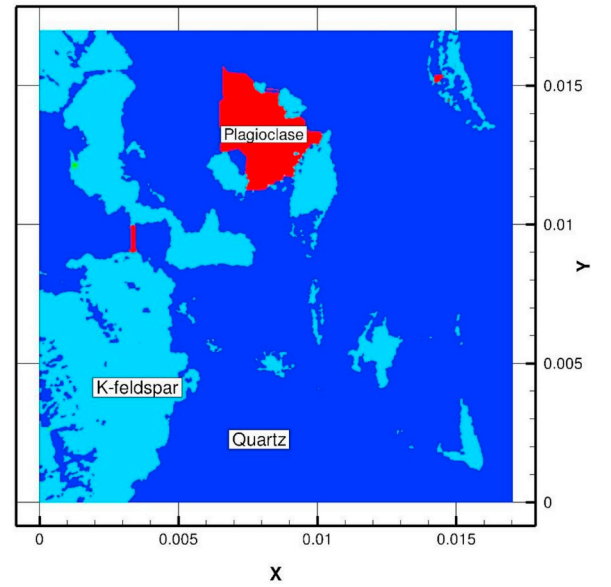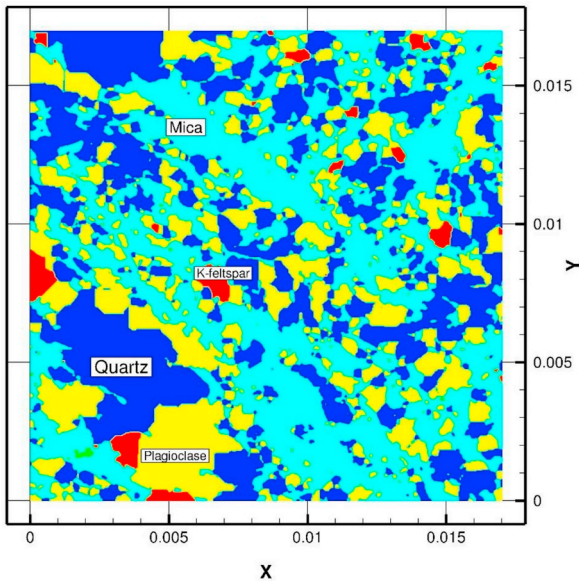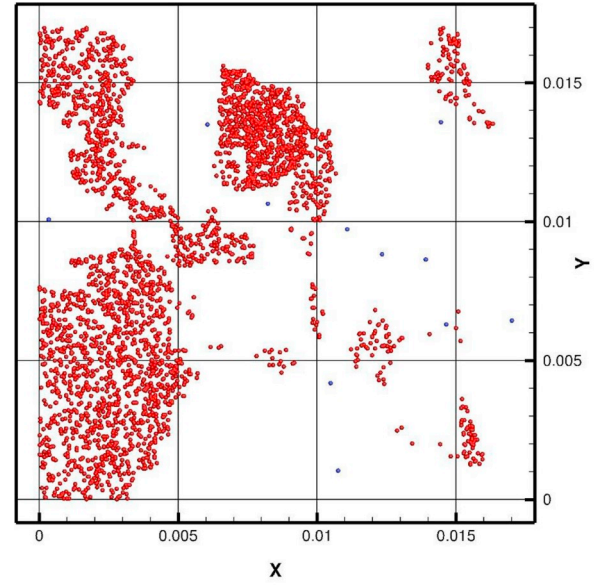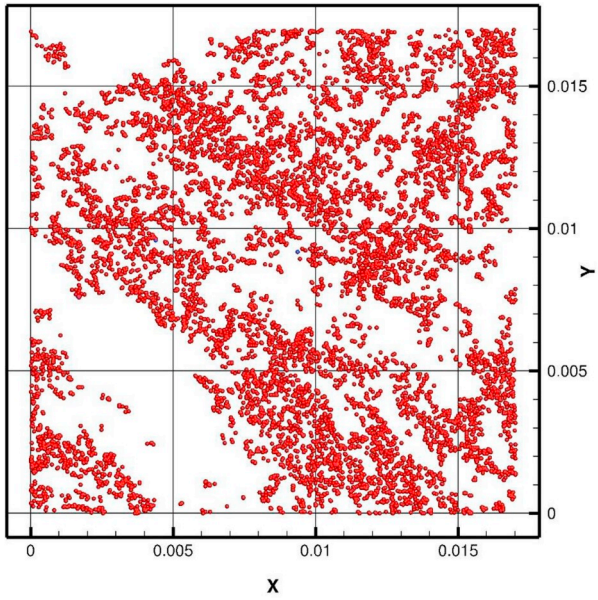
Fig. 13. A particle distribution (top) on the sample surface of VGN in the experiment by Muuri et al., 2018b versus the corresponding mineral distribution of the surface (bottom). Here the particles are only allowed to sorb on mica and this can be seen in the heterogeneous particle distribution.

Fig. 14. A particle distribution (top) on the sample surface of PGR in the experiment by Muuri et al., 2018b versus the corresponding mineral distribution of the surface (bottom). Here the particles are only allowed to sorb on plagioclase and K-feldspar and this can be seen in the heterogeneous particle distribution.

will in this section discuss the relation between K_d and the parameters of the present model.

The K_d value is a direct measure of the partitioning of a tracer between the solid and liquid phases. Values are obtained from laboratory experiments where crushed material is placed in a liquid solution. At equilibrium the amount of the tracer sorbed on the mineral and the amount still in the solution is measured. Let us see how this works out for a particle tracking approach. If we denote the mass of the crushed material by m and the volume of the solute by V, K_d is obtained as:

$$K_d = \frac{N_{sorb}}{N_{free}} \frac{V}{m} \quad [\text{m}^3/kg]$$

(7)

where N_{sorb} and N_{free} are the number of sorbed and free particles, respectively.

In Appendix A, a relation between K_d and the parameters of the present model is derived:

$$K_d = \frac{6 P_s' l_2 T_d}{\rho d T_s}$$

(8)

where ρ is the density of the grain particles, d the diameter of a sphere (the sorbing surface is assumed to be due to spherical grains) and l_2 is the distance from the mineral surface to where a particle has a probability to get sorbed, as explained earlier. The distance l_2 is set to the cell size Δ in a numerical simulation. If we use the same values for P_s', T_s and Δ as in the application to the laboratory experiments we arrive at a relation between K_d and T_d and d; this relation is shown in Fig. 16. A numerical simulation was also performed by simulating the sorption on a cube ($5 \times 5 \times 5 \text{ mm}^3$) placed in a box ($10 \times 10 \times 10 \text{ mm}^3$). At steady state equilibrium N_{sorb} and N_{free} were noted and K_d was calculated from Eq. (7). This confirmed the relations shown in Fig. 16. These relations are useful when considering the connection to experimentally determined, so called batch, K_d values. It should however be remembered that surface sorption at equilibrium is assumed.
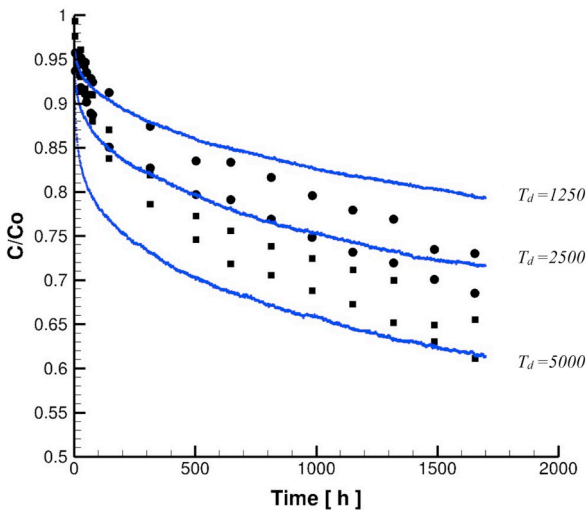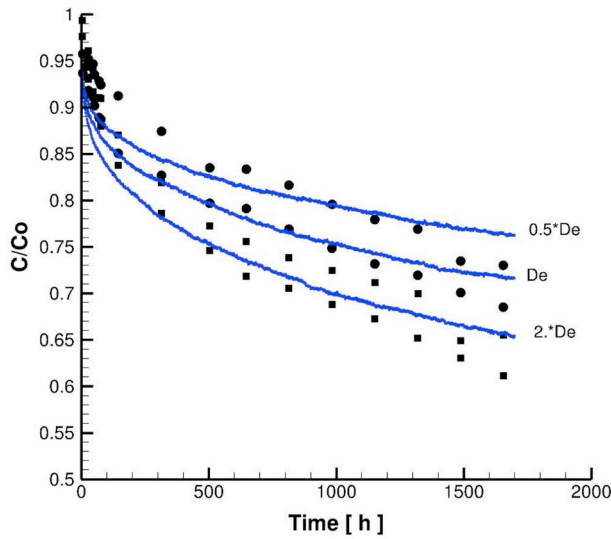
U. Svensson, et al.

Fig. 16. Relation between K_d and T_d for three sphere diameters.

Fig. 15. Sensitivity studies for the case shown in Fig. 10. Effects of changing the effective diffusion coefficient, D_e, (top) and desorption time, T_d, (bottom) with a factor of 2.0 are shown.

Fig. 17. Illustration of the relationship T_d versus K_d for cesium in first case considered (Muuri et al., 2017). The numerical values are given in Table 4.

Table 4

T_d [s] values used in the simulations to fit the experimental data (Figs. 8-10). Corresponding K_d [m^3/kg] values (from Muuri et al., 2017, 2018a) in brackets. For VGN it is assumed that particles sorb only on mica. For PGR it is assumed that particles sorb on plagioclase and K-feldspar, only.

Case	Mineral		
	Mica	Plagioclase	K-feldspar
Cesium, Muuri et al. (2017)	2×10^5 (0.577)	2.5×10^4 (0.0256)	5000 (0.0052)
Barium, Muuri et al., 2018a	7000 (0.084)	6000 (0.009)	2500 (0.0032)
Barium, Muuri et al., 2018b	2500	1200	500

Next, we consider sorption on "inner surfaces". In Appendix B, it is shown how T_d can be related to K_d for a so called through-diffusion case. BTC:s for a VGN sample are generated and compared to an analytical solution. The outcome is:

$$K_d = 2.6 \times 10^{-6} \times T_d$$

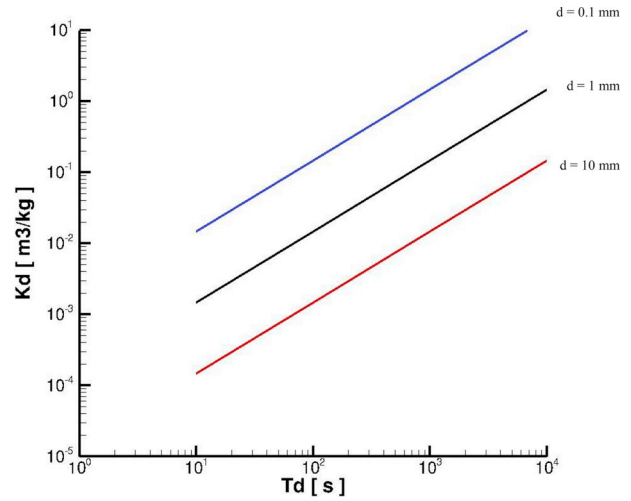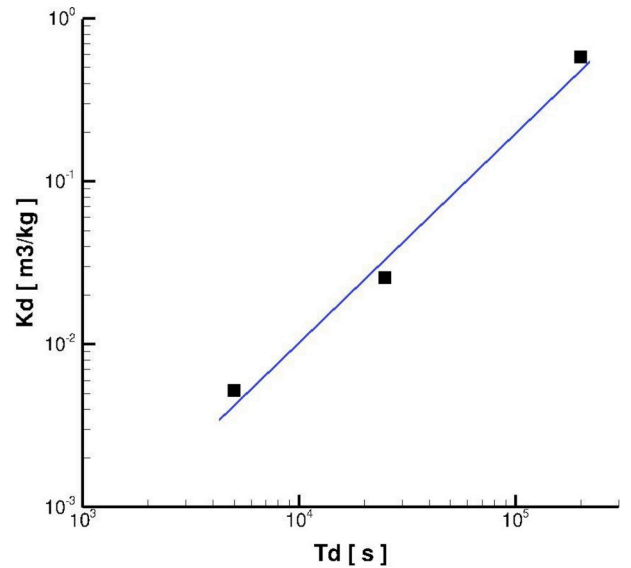It is clear that much smaller K_d values result from this relation, as compared to the "batch experiment values" shown in Fig. 16. This is expected as the internal mineral surfaces are less accessible for the particles.

The laboratory experiments by Muuri et al., 2017, 2018a, 2018b are probably best described as having both surface and internal sorption as important components. The $C(t)/C_0$ curves have a characteristic shape, where the first fast drop is due to surface sorption and the smaller drop later on indicates that penetration takes place. In Muuri et al. (2017) mineral specific K_d values are given. In our model we need mineral specific T_d:s for the radionuclide simulated. The relation between these two parameters is clearly of interest. The relation for cesium is shown in Fig. 17, based on the data given in Table 4.

As a final comment it is noted that the K_d method has several shortcomings:

1. K_d values need to be evaluated for each new rock type, as the mineral abundances are not explicitly accounted for.
2. K_d values may have two contributions, surface sorption and sorption on internal surfaces.
3. K_d values are determined for the crushed material. Crushing creates additional fresh mineral surfaces that may be more reactive than

aged surfaces. Previously, it has been shown that the crushing increases the K_d values by about factor of 10 (André et al., 2009; Muuri et al., 2018b; Puukko et al., 2018; Voutilainen et al., 2019b). Furthermore, K_d values dependent on the size distribution of the crushed material (Lehto et al., 2019).

The suggested method may eliminate some of these shortcomings but requires T_d values for each mineral type for each radionuclide considered; the laboratory data are available for limited number of radionuclides. Other possibility to resolve the shortcomings could be using a model for handling uptake kinetics (Barrow, 1978). This kind of models would be particularly advantageous when speciation of the elements is of interest.

We present the model as an approach to sorption in a rock matrix. It is then in place to discuss assumptions and limitations. One of the key limitations is that we are only considering the intergranular space. For an in-diffusion problem, fractures and grain boundaries may dominate the process. The intragranular domain does however contribute to the total porosity and may also provide sorption sites. In Svensson et al. (2018) alternative ways of generating the intergranular and intragranular domain are illustrated. It is expected that the future development of the model will focus on the inclusion of the intragranular domain.

5. Conclusions

We have presented a particle based numerical reactive transport model that represents reactive grain surfaces explicitly. A three-dimensional mineral map, given by X-μCT, is the starting point. From this a computational grid for the intergranular space is generated and grid properties are generated from a micro-DFN.

The transport model is based on the concept "when a particle is close to a reactive mineral surface it has a probability, P_s, to get sorbed within a time span T_s. Once sorbed it will remain so a certain time, T_d, before desorbed". P_s and T_s are given fixed values, while T_d is considered as a calibration parameter.

The model is evaluated by applications to some recent laboratory experiments by Muuri et al., 2017, 2018a, 2018b. These experiments include two rock types, veined gneiss and pegmatitic granite and two radionuclides, cesium and barium. It is concluded that the model can be tuned to these experimental results, using T_d as the single calibration parameter. Finally, the model parameters are related to the traditional distribution parameters K_d and K_a.

Acknowledgements

Appendix A. The $T_d - K_a$ and $T_d - K_d$ relations at equilibrium

The case considered is shown in Fig. A.1. In a box with one sorbing surface, we study how N particles are distributed at equilibrium (or steady state). Particles can be in solution (n_1), in solution but candidates for sorption (n_2) or sorbed on the surface (n_3). The particles that may be sorbed are located within a distance l_2 from the surface. These particles have a probability, P_s, to get sorbed within a time span T_s. If sorbed the expected time before desorption is T_d.

The following relations apply:

$$N = n_1 + n_2 + n_3 \tag{A1}$$

$$\frac{n_1}{l_1} = \frac{n_2}{l_2} \qquad \text{no concentration gradient in the box} \tag{A2}$$

$$\left. \begin{array}{l} \text{sorbing rate} \quad = n_2 P_s'/T_s \\ \text{desorbing rate} = n_3/T_d \end{array} \right\} \quad n_2 P_s' = n_3 T_s/T_d \tag{A3}$$

where $P_s' = -Log(1 - P_s)$ according to the derivation of Eq. (3).

Eqs. (A1)–(A3) yield:

$$\frac{n_1}{N} = \frac{l_1/l_2}{1 + l_1/l_2 + P_s' T_d/T_s} \tag{A4}$$

$$\frac{n_2}{N} = \frac{1}{1 + l_1/l_2 + P_s' T_d/T_s} \tag{A5}$$

$$\frac{n_3}{N} = \frac{P_s' T_d/T_s}{1 + l_1/l_2 + P_s' T_d/T_s} \tag{A6}$$

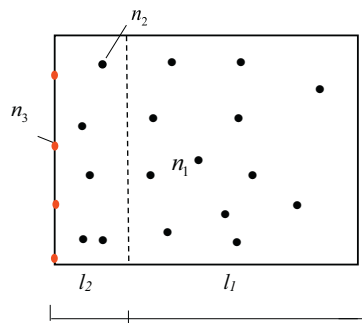These three expressions add up to 1.0, as expected.

Fig. A.1. Outline of the case considered. $N(n_1 + n_2 + n_3)$ particles in a box of length $l_1 + l_2$. Left side of the box is considered to be a sorbing surface.

The surface sorption coefficient, K_a, is defined as the sorbed mass per unit area divided by the mass in solution per unit volume:

$$K_a = \frac{n_3/Area}{(n_1 + n_2)/Vol} \tag{A7}$$

After introduction of (A4)–(A6) we get:

$$K_a = P_s' l_2 T_d / T_s \tag{A8}$$

which is the sought relation.

If we assume that the sorbing surface is due to the surface of a particle, it is possible to relate K_a to K_d. For spherical particles of diameter d the relation is:

$$K_d = \frac{6K_a}{\rho d} \tag{A9}$$

where ρ is the particle density.

This gives:

$$K_d = 6P_s' l_2 T_d / \rho d T_s \tag{A10}$$

which is the sought relation.

Appendix B. The $T_d - K_d$ relation based on a transient through-diffusion analysis

The case considered is shown in Fig. B.1. It is a through-diffusion set-up with constant concentration in the upstream reservoir. The time integrated flux at the downstream boundary, i.e. the breakthrough-curve (BTC), is the main output of interest.

The initial and boundary conditions for the case are as follows:

$$C(x,0) = 0 \quad x \geq 0$$
$$C(0,t) = C_0 \quad t \geq 0$$
$$C(x,t) = 0 \quad x = d$$

where C_0 is the concentration in the reservoir. In accordance with the chosen boundary conditions, the analytical solution of Fick's 2nd law for the contaminant mass, M, that has diffused through the rock slab per unit area is given by (Crank, 1975):

$$M = C_0 \alpha d \left(\frac{D_a t}{d^2} - \frac{1}{6} - \frac{2}{\pi^2} \sum_{n=1}^{\infty} \frac{(-1)^n}{n^2} \exp \left[\frac{-n^2 \pi^2 D_a t}{d^2} \right] \right) \tag{B1}$$

where t is time, D_a apparent diffusion coefficient and α rock capacity.

This solution will be compared with the numerical model, based on a VGN sample ($10 \times 10 \times 10$ mm³) and sorption on mica. We first simulate BTC:s for a range of T_d:s and then fit the analytical solution to these BTC:s by adjusting the apparent diffusion coefficient, D_a. It is then straight forward to find the corresponding K_d by the relation $D_a = D_e/(\varepsilon + \rho K_d)$.

Before the $T_d - K_d$ relation is discussed we need to consider the conservative ($T_d = K_d = 0$) case, as the porosity, ε, and the effective diffusion coefficient, D_e, will be treated as known. From a steady state diffusion simulation, using the VGN sample, it was found that $D_e = 1.7 \times 10^{-13}$ m²/s and $\varepsilon = 0.61\%$. Hence, it is only ρK_d that are not known in the analytical solution; ρ was set to 2700 kg/m³.

For the sorbing cases two more aspects need to be considered. Firstly, we do not want the results to be dominated by surface sorption on the upstream face of the sample. For this reason, the first 50×10^{-6} m of the sample was specified as non-sorbing for all cases. Secondly, the concentration in the upstream reservoir should be constant. For strongly sorbing cases, and hence long integration times, it was required to continuously add particles to the reservoir. By doing so an approximately constant concentration could be preserved.

A range of T_d values (0, 10, 100 and 1000) were then specified and the corresponding BTC:s were generated. The case $T_d = 0$ can be regarded as a limiting case for small sorption rates. From the analytical solution the K_d values that fitted the numerical solution were found; the comparison is shown in Fig. B.2. The K_d values were found to be linearly related to T_d:

$$K_d = 2.6 \times 10^{-6} \times T_d \tag{B2}$$

The simple relation found is encouraging, but it should be recalled that this K_d is relevant for the sample considered. In our basic model it is a K_d relevant for a specific nuclide on a specific mineral surface that is of more interest.
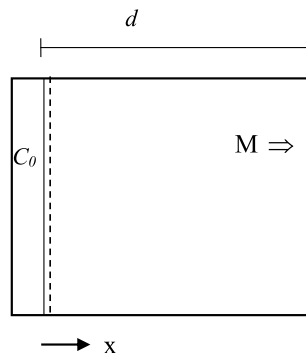

Fig. B.1. Outline of the case considered. The domain has a length of d and the upstream reservoir has a constant concentration C$_0$. The dotted line indicates a distance of 50 μm where sorption is suppressed.
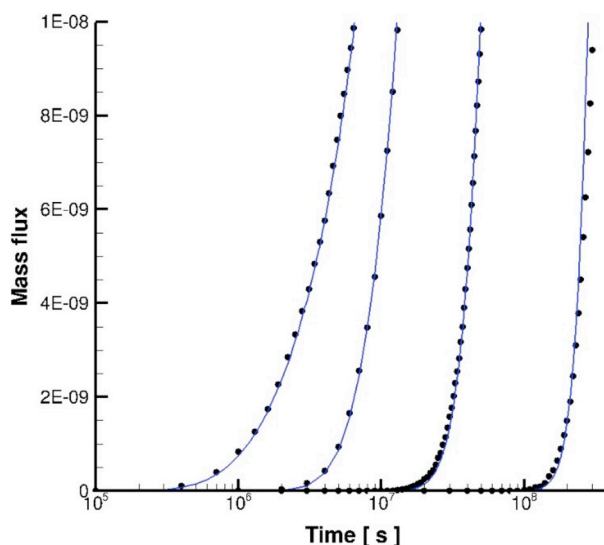
Fig. B.2. Integrated mass flux versus time. Solid lines give the analytical solution and dots the numerical solution. The T_d values specified (from left to right) are: 0, 10., 100. and 1000.

References

André, M., Malmström, M.E., Neretnieks, I., 2009. Determination of sorption properties of intact rock samples: new methods based on electromigration. J. Contam. Hydrol. 103, 71–81. https://doi.org/10.1016/j.jconhyd.2008.09.006.

Aromaa, H., Voutilainen, M., Ikonen, J., Yli-Kaila, M., Poteri, A., Siitari-Kauppi, M., 2019. Through diffusion experiments to study the diffusion and sorption of HTO, ^{36}Cl, ^{133}Ba and ^{134}Cs in crystalline rock. J. Contam. Hydrol. 222, 101–111. https://doi.org/10.1016/j.jconhyd.2019.03.002.

Barrow, N.J., 1978. The description of phosphate adsorption curves. J. Soil Sci. 29 (4), 447–465. https://doi.org/10.1111/j.1365-2389.1978.tb00794.x.

Crank, J., 1975. The Mathematics of Diffusion, 2nd edition. Oxford University press, London.

Dentz, M., Gouze, P., Russian, A., Dweik, J., Delay, F., 2012. Diffusion and trapping in heterogeneous media: An inhomogeneous continu-ous time random walk approach. Adv. Water Resour. 15 (1), 13–22. https://doi.org/10.1016/j.advwatres.2012.07.015.

Fusseis, F., Xiao, X., Schrank, C., De Carlo, F., 2014. A brief guide to synchrotron radiation-based microtomography in (structural) geology and rock mechanics. J. Struct. Geol. 65, 1–16. https://doi.org/10.1016/j.isa.2014.02.005.

Ikonen, J., Sammaljärvi, J., Siitari-Kauppi, M., Voutilainen, M., Lindberg, A., Kuva, J., Timonen, J., 2014. Investigation of rock matrix retention properties. Supporting laboratory studies I: mineralogy, porosity and pore structure. In: Posiva Working Report 2014–68. Posiva Oy, Eurajoki, Finland.

Iraola, A., Trinchero, P., Voutilainen, M., Gylling, B., Selroos, J.-O., Molinero, J., Svensson, U., Bosbach, D., Deissmann, G., 2017. Microtomography-based Inter-Granular Network for the simulation of radionuclide diffusion and sorption in a granitic rock. J. Contam. Hydrol. 207, 8–16. https://doi.org/10.1016/j.jconhyd.2017.10.003.

Kärki, A., Paulamäki, S., 2006. Petrology of Olkiluoto. In: Posiva Working Report 2006–02. Posiva Oy, Eurajoki, Finland.

Ketcham, R., Carlson, W., 2001. Acquisition, optimization and interpretation of X-ray computed tomographic imagery: Applications to the geosciences. Comput. Geosci. 27, 381–400. https://doi.org/10.1016/S0098-3004(00)00116-3.

Kuva, J., Voutilainen, M., Kekäläinen, P., Siitari-Kauppi, M., Timonen, J., Koskinen, L., 2015. Gas phase measurements of porosity, diffusion coefficient, and permeability in rock samples from Olkiluoto bedrock, Finland. Transport Porous Med. 107, 187–204. https://doi.org/10.1007/s11242-014-0432-2.

Kuva, J., Voutilainen, M., Mattila, K., 2019. Modeling mass transfer in fracture flows with the time domain-random walk method. Computat. Geosci. https://doi.org/10.1007/s10596-019-09852-5.

Lehto, J., Puukko, E., Lindberg, A., Voutilainen, M., 2019. Batch sorption experiments of cesium and strontium on crushed rock and biotite for the estimation of distribution coefficients on intact crystalline rock. Heliyon 5 (8), e02296. https://doi.org/10.1016/j.heliyon.2019.e02296.

Molins, S., 2015. Reactive interfaces in direct numerical simulation of pore scale processes. Rev. Mineral. Geochem. 80, 461–481. https://doi.org/10.2138/rmg.2015.80.14.

Muuri, E., Matara-aho, M., Puhakka, E., Ikonen, J., Martin, A., Koskinen, L., Siitari-Kauppi, M., 2018a. The sorption and diffusion of ^{133}Ba in crushed and intact granitic rocks from the Olkiluoto and Grimsel in-situ test sites. Appl. Geochem. 89, 138–149. https://doi.org/10.1016/j.apgeochem.2017.12.004.

Muuri, E., Siitari-Kauppi, M., Matara -aho, M., Ikonen, J., Lindberg, A., Qian, L., Koskinen, L., 2017. Cesium sorption and diffusion on crystalline rock: Olkiluoto case study. J. Radioanal. Nucl. Chem. 311, 439–446. https://doi.org/10.1007/s10967-016-5087-8.

Muuri, E., Sorokina, T., Garcia, D., Grive, M., Bruno, J., Koskinen, L., Martin, A., Siitari-Kauppi, M., 2018b. The diffusion of ^{133}Ba in granitic rock cubes from the Olkiluoto and Grimsel in-situ test sites. Appl. Geochem. 92, 188–195. https://doi.org/10.1016/j.apgeochem.2018.03.011.

Posiva, 2013. Safety case for the disposal of spent nuclear fuel at Olkiluoto – Models and data for the repository system 2012. In: Posiva Report 2013–01. Posiva Oy, Eurajoki, Finland.

Puukko, E., Lehto, J., Lindberg, A., Voutilainen, M., 2018. Electromigration experiments for studying transport parameters and sorption of cesium and strontium on intact crystalline rock. J. Contam. Hydrol. 217, 1–7. https://doi.org/10.1016/j.jconhyd.2018.08.010.

Russian, A., Dentz, M., Gouze, P., 2016. Time Domain Random Walks for hydrodynamic transport in heterogeneous media. Water Resour. Res. 52, 3309–3323. https://doi.org/10.1002/2015WR018511.

Sammaljärvi, J., Lindberg, A., Voutilainen, M., Ikonen, J., Siitari-Kauppi, M., Pitkänen, P., Koskinen, L., 2017. Multi-scale study of the mineral porosity of veined gneiss and pegmatitic granite from Olkiluoto, Western Finland. J. Radioanal. Nucl. Chem. 314, 1557–1575. https://doi.org/10.1007/s10967-017-5530-5.

Smellie, J., Pitkänen, P., Koskinen, L., Aaltonen, I., Eichinger, F., Waber, N., Sahlstedt, E., Siitari-Kauppi, M., Karhu, J., Löfman, J., Poteri, A., 2014. Evolution of the Olkiluoto site: Palaeohydrogeochemical considerations. In: Posiva Working Report 2014–27. Posiva Oy, Eurajoki, Finland.

Svensson, U., Ferry, M., 2014. DarcyTools: A computer code for hydrogeological analysis of nuclear waste repositories in fractured rock. J. Appl. Math. Phys. 2, 365–383. https://doi.org/10.4236/jamp.2014.26044.

Svensson, U., Löfgren, M., Trinchero, P., Selroos, J.-O., 2018. Modelling the diffusion-available pore space of an unaltered granitic rock matrix using a micro-DFN approach. J. Hydrol. 559, 182–191. https://doi.org/10.1016/j.jhydrol.2018.02.041.

Svensson, U., Trinchero, P., Ferry, M., Voutilainen, M., Gylling, B., Selroos, J.-O., 2019. Grains, grids and mineral surfaces. -Approaches to grain scale matrix modelling based on X- ray micro computed tomography data. (Submitted to publication).

Tachi, Y., Ito, T., Akagi, Y., Satoh, H., Martin, A., 2018. Effects of fine-scale surface alterations on tracer retention in a fractured crystalline rock from the Grimsel Test Site. Water Resour. Res. 54 (11), 9287–9305. https://doi.org/10.1029/2018WR023145.

Trinchero, P., Painter, S., Ebrahimi, H., Koskinen, L., Molinero, J., Selroos, J.-O., 2016. Modelling radionuclide transport in fractured media with a dynamic update of Kd values. Comput. Geosci. 86, 55–63. https://doi.org/10.1016/j.cageo.2015.10.005.

Voutilainen, M., Miettinen, A., Sardini, P., Parkkonen, J., Sammaljärvi, J., Sardini, P., Gylling, B., Selroos, J.-O., Yli-Kaila, M., Koskinen, L., Siitari-Kauppi, M., 2019a. Characterization of spatial porosity and mineral distribution of crystalline rock using X-ray micro computed tomography, C-14-PMMA autoradiography and scanning electron microscopy. Appl. Geochem. 101, 50–61. https://doi.org/10.1016/j.apgeochem.2018.12.024.

Voutilainen, M., Siitari-Kauppi, M., Sardini, P., Lindberg, A., Timonen, J., 2012. Pore-space characterization of an altered tonalite by X-raycomputed microtomography and the14C-labeled-polymethylmethacrylate method. J. Geophys. Res. 117, B01201. https://doi.org/10.1029/2011JB008622.

Voutilainen, M., Kekäläinen, P., Poteri, A., Siitari-Kauppi, M., Helariutta, K., Andersson, P., Nilsson, K., Byegård, J., Skålberg, M., Yli-Kaila, M., Koskinen, L., 2019b.

Comparison of water phase diffusion experiments in laboratory and in situ conditions. J. Hydrol. 575, 716–729. https://doi.org/10.1016/j.jhydrol.2019.05.069.

Voutilainen, M., Kekäläinen, P., Siitari-Kauppi, M., Sardini, P., Muuri, E., Timonen, J., Martin, A., 2017. Modeling transport of celsium in Grimsel granodiorite with micrometer scale heterogeneities and dynamic update of Kd. Water Resour. Res. 53, 9245–9265. https://doi.org/10.1002/2017WR020695.

Voutilainen, M., Ikonen, J., Sammaljärvi, J., Siitari-Kauppi, M., Lindberg, A., Kuva, J., Timonen, J., Löfgren, M., 2018. Investigation of rock matrix retention properties - supporting laboratories studies II: diffusion coefficient and permeability. In: Posiva Working Report 2017–39. Posiva Oy, Eurajoki, Finland.